Experimental Study on W-Band (75 - 110 GHz) Oversized Surface Wave Oscillator Driven by Weakly Relativistic Electron Beams*)

Min Thu SAN, Kazuo OGURA, Kiyoyuki YAMBE, Yuta ANNAKA, Shaoyan GONG, Jun KAWAMURA, Takuro MIURA, Shin KUBO[1)], Takashi SHIMOZUMA[1)], Sakuji KOBAYASHI[1)] and Kohji OKADA[1)]

Graduate School of Science and Technology, Niigata University, Niigata 950-2181, Japan
[1)]*National Institute for Fusion Science, 322-6 Oroshi-cho, Toki 509-5292, Japan*

(Received 27 November 2015 / Accepted 2 April 2016)

A W-band (75 - 110 GHz) oversized surface wave oscillator driven by weakly relativistic electron beams with energy in the range of 10 - 80 keV is studied. Rectangular corrugations are used as slow-wave structures (SWS) having surface waves with an upper cutoff frequency of approximately 100 GHz (W-band). Uniformly distributed annular electron beams are generated by a disk-type cold cathode and then are injected into the W-band oscillator. A longer SWS length causes the oscillator to function in both backward wave oscillator (BWO) and travelling wave tube (TWT) operations, and no meaningful oscillation occurs at the π-point or the Bragg condition. When the SWS length is short enough, oscillation occurs in all regions: BWO, π-point and TWT. The operations of the oscillator are strongly affected by the structure length. The maximum radiation power is estimated to be approximately 20 kW with the figure of merit of about 2×10^2 MW.GHz^2.

Keywords: surface wave, travelling wave tube operation, backward wave oscillator operation, π-point, W-band

DOI: 10.1585/pfr.11.2406085

1. Introduction

High-power microwaves are required for a variety of applications, such as plasma heating, plasma diagnostics, and radar systems. Slow-wave devices, such as backward wave oscillators (BWOs) have been extensively studied as candidates for high- and moderate-power microwave sources. In these devices, a slow-wave structure (SWS) is used to generate slow waves by reducing the phase velocity of electromagnetic waves to the beam velocity. For high-frequency operations in the terahertz frequency range (0.1 - 10 THz), oversized SWSs with diameter much larger than the free-space wavelength of the electromagnetic waves are suitable. The relativistic diffraction generator and the multi-wave Cherenkov generator are special versions of oversized BWOs, and have produced peak powers above GW levels in the frequency range of up to approximately 46 GHz (Q-band) [1, 2]. Such tremendously high-power devices use relativistic MV level pulsed power systems and Tesla level magnetic field systems. For practical applications, operations at reduced voltages and reduced magnetic fields are preferable. In Ref. 3, a power level of approximately 500 MW was achieved at 8.3 GHz (X-band) by reducing voltage to approximately 500 kV. However, this system still requires a bulky pulsed power system. For lower voltage operations, the phase velocity of the electromagnetic wave in a SWS should be reduced, e.g., 0.55c for 100 kV. Designing of the oversized SWSs to enable the transmission of electromagnetic waves with such a slow phase velocity is difficult because high-frequency operations and lower voltage operations are incompatible.

Aiming at more compact devices, oversized BWOs operating in weakly relativistic regions less than 100 kV have been studied in the K- and Q-band by using uniformly distributed annular electron beams [4–6]. An annular beam of the order of 100 A completely covers the corrugated surface. Recently, the performance of the weakly relativistic oversized BWO has been improved, and radiation of up to 500 kW (K-band) and 200 kW (Q-band) has been achieved [5]. The radiation power level of kW has been implemented above 150 GHz (G-band) with a moderate voltage of less than 100 kV [7, 8]. The unique features of these oversized BWOs are as follows: (1) the use of a cold cathode to obtain a uniformly distributed annular electron beam [9, 10], (2) operation by a weakly relativistic electron beam of less than 100 kV, and (3) a guiding magnetic field of less than 1.0 T.

The interaction of the beam and the electromagnetic wave in SWSs may result in backward wave or travelling wave operations, depending on the group velocity of the surface wave, as shown in Fig. 2. At high electron energy, the group velocity of this wave is positive and the device operates in the manner of a travelling wave tube (TWT). At low electron energy, the group velocity is negative and operates as a BWO. In addition, at an intermediate energy,

author's e-mail: minthusan1@gmail.com

*) This article is based on the presentation at the 25th International Toki Conference (ITC25).

known as the Bragg condition or π-point, the group velocity of the evanescent wave vanishes. The overall operation from BWO to TWT has been studied theoretically and it has been shown that there is no operation near the π-point [11]. To date, the theoretical prediction has not been validated against experimental results.

The operation mechanism for the surface wave oscillator is still open, and a comparison between theories and experiments of the oscillator is very important to develop a high-frequency surface wave oscillator. It is commonly believed that the operation of BWO occurs due to the absolute instability at the saddle point formed by the beam mode and the backward surface wave. However, for a finite-length BWO, the axial boundary conditions caused by the reflection at both ends should be considered. The finite length effect results in a new idea of the so-called "axial mode" or "surface wave cavity" which is a type of cavity formed by the reflected surface waves. In addition, the surface wave cavity has been demonstrated to generate intense terahertz radiation in the BWO region [7,8]. A surface wave cavity in the TWT region may also be available in realistic devices. However, such a cavity has not been studied to date.

Here we studied a W-band oversized surface wave oscillator based on the surface wave cavity driven by weakly relativistic electron beams. In this paper, the W-band refers to the frequency range from 75 to 110 GHz of the Electronic Industries Alliance (EIA) standard WR-10 rectangular waveguide [12]. The oversized oscillator uses a SWS that forms surface waves with an upper cutoff frequency of approximately 100 GHz. The SWS is designed so that the BWO and TWT operations are realized by weakly relativistic beams. The π-point operation occurs for the beam at approximately 30 kV, shown in Fig. 2, at which the phase velocity of the surface wave should be $0.33c$. By varying the beam voltage from 10 to 80 kV, the phase velocity of surface wave varies from $0.20c$ to $0.50c$, and the overall operation from BWO to TWT can be realized. To examine the finite length effect on the surface wave oscillation, the SWS length is varied as 40, 80, and 120 periods.

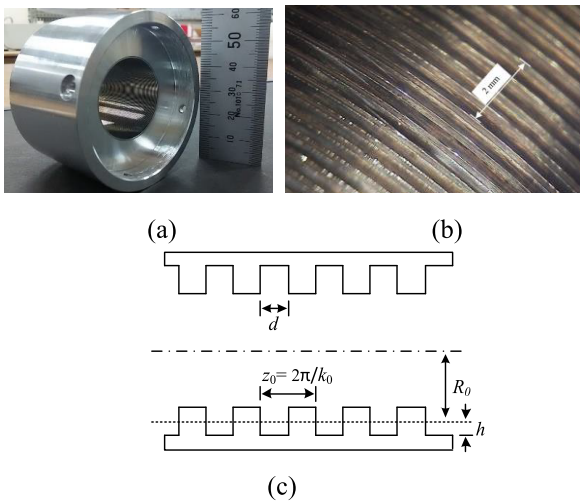

Fig. 1 (a) One modular section of the W-band corrugated hollow waveguide with length $L = 80z_0$. (b) Enlarged photo of the rectangular corrugation. (c) Size parameters of the rectangular corrugation R_0, h, d, and z_0.

Table 1 Parameters of W-band Corrugation.

R_0 (mm)	h (mm)	d (mm)	z_0 (mm)
15.1	0.3	0.3	0.5

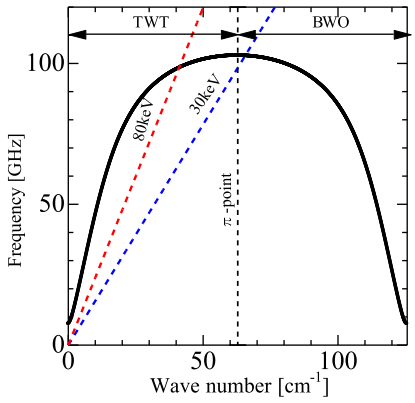

Fig. 2 Dispersion curve of W-band oscillator with 30 and 80 keV beam lines.

2. W-Band SWS

The W-band SWS used in this work is the oversized hollow waveguide with outer corrugation shown in Figs. 1 (a) and (b). The SWS is made of aluminum and fabricated by machining and has eighty periods ($80z_0$). The size parameters of the rectangular corrugation shown in Fig. 1 (c) are the average radius R_0, the corrugation amplitude h, the corrugation width d, and the periodic length z_0. The corrugation wave number is given by $k_0 = 2\pi/z_0$. The dispersion characteristics of the SWS are controlled by changing R_0, h, d, and z_0. Table 1 presents the SWS corrugation parameters used in the experiment. For these parameters of corrugation, the electric field is concentrated in a very narrow region within approximately 0.5 mm from the SWS wall near the π-point, and the surface waves are formed. Two modular sections of the oversized SWS are used: one has eighty periods ($80z_0$), and the other one has forty periods ($40z_0$). The lengths of the SWSs used in the experiment are of $40z_0$, $80z_0$, and $120z_0$. The last one is obtained by combing the two modules.

The dispersion curves of the rectangular SWS are obtained by a numerical method based on the mathematical formula in [12–14]. Figure 2 shows the dispersion curve of TM_{01} mode for W-band oversized oscillator. According to Floquet's theorem, the curve is periodic in wave number space (k_z-space) with a period of $k_0 = 126\,\mathrm{cm}^{-1}$ and has an upper cutoff frequency of approximately 100 GHz

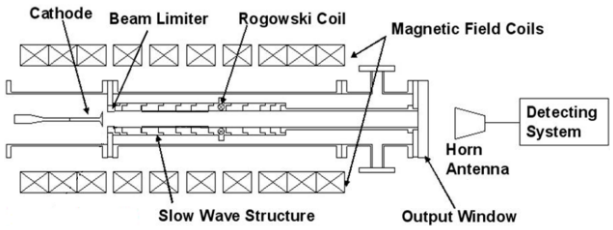

Fig. 3 Schematic diagram of the experimental set-up.

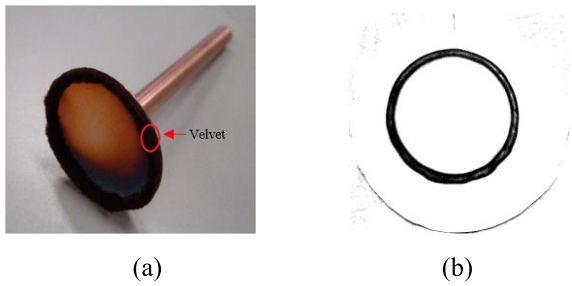

Fig. 4 Disk-type cold cathode with velvet at the outer surface. (b) Burn pattern of the electron beam.

at the π-point, with $k_z = k_0/2$. The TM_{01} mode is a surface wave in the slow-wave region with a phase velocity less than the light velocity, and the dispersion curve is flat around the upper cutoff. In addition, the interaction point between the beam line of the slow space charge mode and the TM_{01} mode shifts toward the TWT region at 80 keV, and with decreasing beam energy to 30 keV, the interaction point moves to the BWO region. At approximately 30 keV, the interaction point is at the π-point.

3. Experimental Set-Up

A schematic of the experimental set-up is shown in Fig. 3. An output voltage of up to 80 kV from a pulse forming line (PFL) is applied to a disk-type cold cathode, which is shown in Fig. 4 (a). The cathode is made of oxygen free copper, and its diameter is 29 mm. In order to obtain a uniform electron beam, a velvet band is attached to the axisymmetric emitting edge of the cathode. By adjusting the velvet band, fairly uniform annular beams are obtained. The beam limiter with a diameter of 29.7 mm is placed at the entrance of the waveguide to prevent the erosion of the corrugation by the high-energy beams. Uniform annular beams in the weakly relativistic region are obtained with nearly the same diameter as that of the cathode. The inner and outer diameters of the annular electron beam shown in Fig. 4 (b) are 26 and 30 mm, and the thickness of the beam is typically 2 - 3 mm. For beam propagation, a uniform axial magnetic field is provided by 10 solenoid coils. The value of the magnetic field can be changed from zero to approximately 1 T; the field is 0.82 T in this study. The microwave output is picked up by rectangular horn antennas of F- and G-bands, which are EIA standard rectangular waveguides with cutoff frequencies of 74 and 116 GHz [15], respectively, located typically 600 mm away from the output window. After providing an adequate amount of attenuation, the output powers are detected by crystal detectors.

4. Experimental Results

Typical waveforms of the W-band oversized oscillator with 40-period SWS length are shown in Fig. 5. The microwave signals are detected by the F-band (90 - 140 GHz) rectangular horn antenna with 10 dB attenuation, and the G-band (140 - 220 GHz) rectangular horn antenna

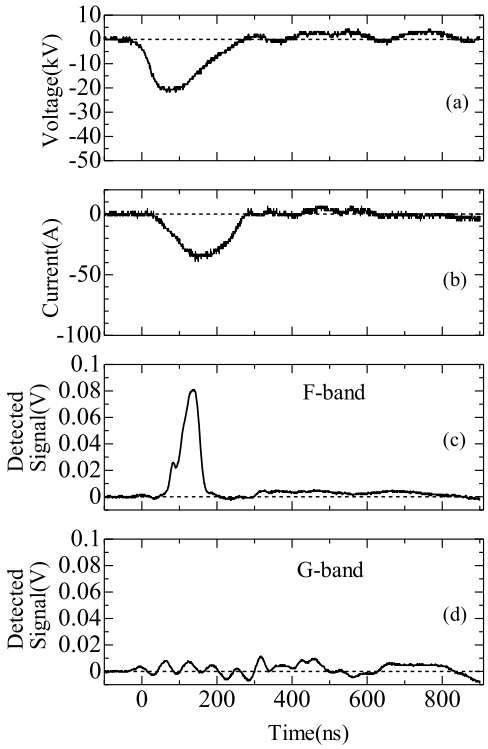

Fig. 5 Waveforms of the measured signals: (a) beam voltage, (b) beam current, (c) detected signal by F-band antenna, and (d) detected signal by G-band antenna.

with 0 dB attenuation, at a position of 600 mm away from the output window. We evaluated the detected powers using the F-band voltage signals, which are calibrated to absolute powers by using a Gunn oscillator at 100 GHz.

Figure 5 (c) shows that the microwave signal is detected by the F-band antenna. However, no meaningful signal is detected by the G-band antenna, as shown in Fig. 5 (d). The operation frequency is examined using rectangular waveguides with various cutoff frequencies. We used F-band and G-band waveguides as high-pass filters with cutoff frequencies of 74 and 116 GHz, respectively. Figure 6 shows the dependence of the microwave power on the beam voltage for the SWS length of 40 periods. In the experiment, the voltage and current change with time, and their values at the time of the microwave peak are plotted.

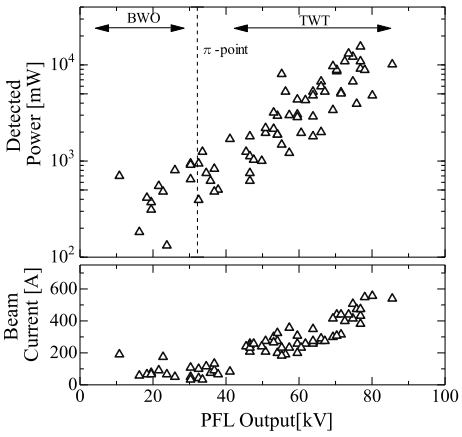

Fig. 6 Peak value of the W-band signal and beam current versus beam voltage for the SWS length of 40 periods. The beam voltages at the radiation peaks are used. The magnetic field is approximately 0.82 T.

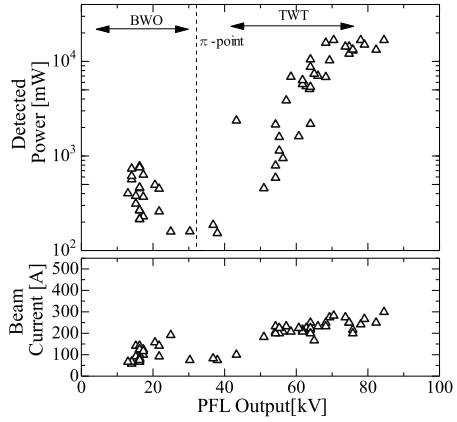

Fig. 7 Peak value of the W-band signal and beam current versus beam voltage for the SWS length of 80 periods. The beam voltages at the radiation peaks are used. The magnetic field is approximately 0.82 T.

The oscillation starting voltage is approximately 10 kV. No meaningful output power is detected for the beam voltage of less than 10 kV. Output powers increase by increasing the beam voltage. The microwave output powers can be detected until the beam voltage of approximately 80 kV. The oscillations occur through the beam voltage of 10 - 80 kV. As shown in Fig. 2, the beam interaction point with TM_{01} is in BWO region while the beam energy is under approximately 30 keV. When the beam energy is above 30 keV, the interaction is near to the π-point. In addition, even near the π-point, meaningful microwave output signals are detected, as shown in Fig. 6. By increasing the beam energy up to 80 keV, the interaction point between the slow space charge mode and the TM_{01} mode shifts toward the TWT region.

Microwave signals and beam currents versus beam voltages for SWS lengths of 80 and 120 periods are shown in Figs. 7 and 8, respectively. Radiation is clearly detected

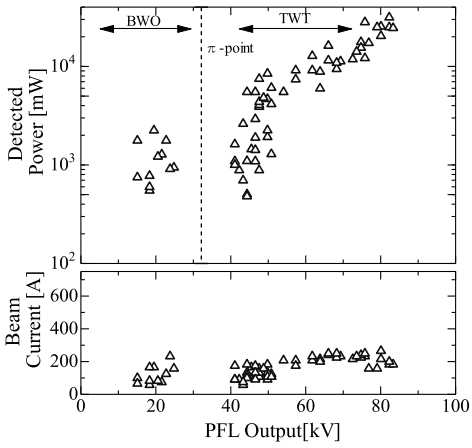

Fig. 8 Peak value of the W-band signal and beam current versus beam voltage for the SWS length of 120 periods. The beam voltages at the radiation peaks are used. The magnetic field is approximately 0.82 T.

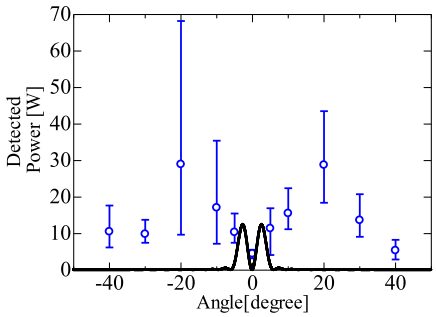

Fig. 9 Radiation pattern for the TWT operation of the 80-period SWS length. The operating parameters are approximately 70 kV, 200 A and 0.82 T. The solid curve is the calculated radiation pattern for the TM_{01} waveguide mode.

within the range of beam voltages approximately 10 and 25 kV. Meaningful radiation disappears within the range of beam voltages of 25 and 40 kV. In addition, the microwave outputs are observed again above 40 kV and increase in accordance with the beam voltage increment up to about 80 kV. In Figs. 7 and 8, at the starting energy of approximately 10 keV, the interaction point is in the BWO. Increasing the beam energy from 25 to 40 keV, the beam interaction point with TM_{01} is close to the upper cutoff at the π-point, as shown in Fig. 2. Over the beam energy of 40 keV, the interaction point moves into the TWT region.

In order to examine the mode, the radiation patterns were obtained by moving a receiving horn antenna in an equatorial plane around a pivot at the center of the output window. The horizontal components of the electric field were measured. The pattern for TWT operation of the 80-period SWS length is shown in Fig. 9. As a reference, a theoretical radiation curve for the TM_{01} waveguide mode is shown. The measured pattern appears to be axisymmetric with a dip at the center. The pattern is broad and cannot be explained by a single TM_{01} mode. Higher order

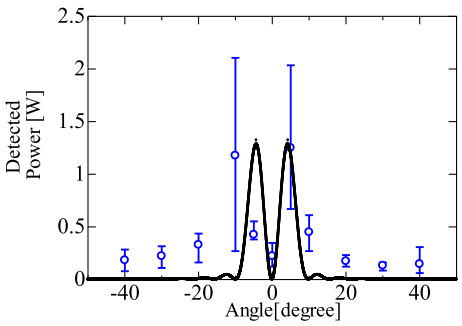

Fig. 10 Radiation pattern for the π-point operation of the 40-period SWS length. The operating parameters are approximately 30 kV, 150 A and 0.82 T. The solid curve is the calculated radiation pattern for the TM_{01} waveguide mode.

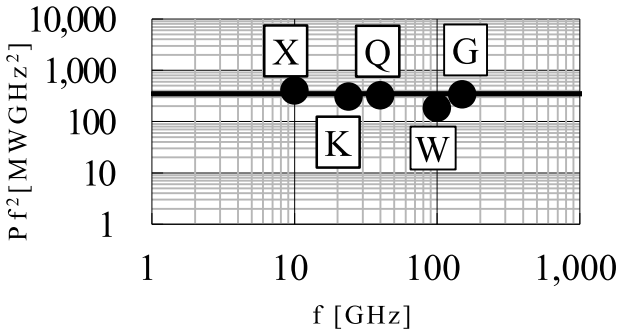

Fig. 11 Figure of merits of X-, K-, Q-, W- and G-band oscillators based on the oversized SWS.

waveguide modes are required to explain this broad radiation. The radiation patterns for the BWO operation are also broad, as shown in Fig. 9. The W-band oversized surface wave oscillator is found to be a multimode system in the BWO and TWT regions, and many modes may be excited simultaneously.

The radiation pattern for π-point operation of the 40-period SWS length is shown in Fig. 10. The operating parameters are approximately 30 kV, 150 A and 0.82 T. In this case, the radiation pattern approaches the TM_{01} mode. In other words, the higher order modes in the multimode system are suppressed around the π-point and the oscillation approaches a single mode operation.

The maximum detected power is observed in the TWT region, as shown in Fig. 8, at approximately 80 kV. By integrating the detected power over the broad pattern, the corresponding maximum radiation power is estimated to be approximately 20 kW.

5. Discussion and Conclusion

The performance of the W-band oversized surface wave oscillator is compared with that of the previous K-, Q-, and G-band oversized BWOs driven by an annular beam with energy less than 100 keV. The radiation powers of the K-, Q-, and G-band oversized BWOs are approximately 500, 200 and 15 kW, respectively [5, 7, 8]. The figure of merit of the BWO is approximately 3.5×10^2 MW.GHz^2, as shown in Fig. 11. Here, P is the radiation power, and f is the frequency. For the W-band oversized surface oscillator, the maximum radiation power is approximately 20 kW with the figure of merit of about 2×10^2 MW.GHz^2, which is nearly the same as the previously obtained ones of the BWO as shown in Fig. 11. Note that the figure of merit of the W-band oscillator based on the surface wave cavity in the TWT region has nearly the same value as those of the BWOs.

Here the uniqueness and usefulness of the π-point operation are discussed. In general, oversized SWSs are a multimode system. The presented W-band oversized surface wave oscillator also has a multimode nature and radiates many modes in the BWO and TWT regions. To date, operations near the π-point have not been studied well. Our experiments show that the radiations from the W-band oscillator disappear for the long SWS length of 120 periods. This disappearance qualitatively agrees with a theoretical prediction in [11]. Moreover, we demonstrate that the π-point operation is possible by shortening the SWS length. This π-point operation has a single mode nature; this is a unique and useful result, which may provide one possible solution for the mode competition problem. Mode control is a very difficult problem. To solve this problem, double SWSs are usually examined [16, 17]. The π-point operation presented may give an alternative way to control the operation mode.

In conclusion, we experimentally studied the operation of a W-band oversized surface wave oscillator driven by weakly relativistic electron beams. The microwave output signals and the starting beam energies have nearly the same values for various SWS lengths. The interactions in the BWO and TWT regions are pronounced for longer SWS lengths. At the π-point, meaningful radiation is not detected for the long SWS length. The microwave signals with a sufficiently short SWS length are observed from the π-point operation as well as the BWO and TWT operations. Therefore, the length of the SWS of the oscillator must to be considered for the operation of the W-band oscillator. The W-band oscillator includes a compact terahertz microwave power source with the output microwave power of some tens kW in the weakly relativistic region. The oscillator may be of considerable interest for practical use and for developing compact tunable THz wave sources.

Acknowledgement

This work was partially supported by NIFS Collaboration Research Program Nos. NIFS12KLER014 and NIFS14KLER031.

[1] S.P. Bugaev *et al.*, IEEE Trans. Plasma Sci. **18**, 518 (1990).
[2] S.P. Bugaev *et al.*, IEEE Trans. Plasma Sci. **18**, 525 (1990).

[3] A.N. Vlasov *et al.*, IEEE Trans. Plasma Sci. **28**, 550 (2000).
[4] K. Ogura *et al.*, IEEJ Trans. FM **125**, 733 (2005).
[5] S. Aoyama *et al.*, Trans Fusion Sci. Technol. **51**, 325 (2007).
[6] K. Ogura *et al.*, IEEJ Trans. FM **127**, 681 (2007).
[7] S. Magori *et al.*, Plasma Fusion Res. **9**, 3406032 (2014).
[8] S. Gong *et al.*, IEEE Trans. Plasma Sci. **43**, 3530 (2015).
[9] H. Oe *et al.*, J. Plasma Fusion Res. SERIES **8**, 1477 (2009).
[10] K. Yambe *et al.*, IEEE Trans. Plasma Sci. **41**, 2781 (2013).
[11] H.L. Andrews *et al.*, Phys. Rev. ST Accel. Beams **8**, 050703 (2005).
[12] D.M. Pozar, *Microwave Engineering*, 4th ed. New York, NY, USA: Wiley, (2012), p. 720.
[13] Y. Takashima *et al.*, J. Plasma Fusion Res. SERIES **8**, 1512 (2009).
[14] K. Ogura *et al.*, IEEE Trans. Plasma Sci. **41**, 2729 (2013).
[15] K. Ogura *et al.*, Plasma Fusion Res. **9**, 3406022 (2014).
[16] K. Mizuno *et al.*, IEEE Trans. Electron Devices **ED-20**, 749 (1973).
[17] I.V. Konoplev *et al.*, Phys. Rev. E **76**, 056406 (2007).